Spontaneous 2-Dimensional Carrier Confinement at the n-Type $SrTiO_3/LaAlO_3$ Interface

Pietro Delugas, Alessio Filippetti, and Vincenzo Fiorentini
CNR-IOM UOS Cagliari, Dipartimento di Fisica, Università di Cagliari, SP Monserrato-Sestu km.0.700, 09042 Monserrato (CA), Italy

Daniel I. Bilc, Denis Fontaine, and Philippe Ghosez
Physique Théorique des Matériaux, Université de Liège, Allée du 6 Août 17 (B5), 4000 Sart Tilman, Belgium
(Received 22 December 2010; published 21 April 2011)

We describe the intrinsic mechanism of 2-dimensional electron confinement at the n-type $SrTiO_3/LaAlO_3$ interface as a function of the sheet carrier density n_s via advanced first-principles calculations. Electrons localize spontaneously in Ti $3d_{xy}$ levels within a thin ($\lesssim 2$ nm) interface-adjacent $SrTiO_3$ region for n_s lower than a threshold value $n_c \sim 10^{14}$ cm^{-2}. For $n_s > n_c$ a portion of charge flows into Ti $3d_{xz}$-d_{yz} levels extending farther from the interface. This intrinsic confinement can be attributed to the interface-induced symmetry breaking and localized nature of Ti $3d$ t_{2g} states. The sheet carrier density directly controls the binding energy and the spatial extension of the conductive region. A direct, quantitative relation of these quantities with n_s is provided.

DOI: 10.1103/PhysRevLett.106.166807 PACS numbers: 73.20.−r, 71.15.−m, 72.15.Rn

Several years of intensive research have not yet led to a univocal explanation of the surprising two-dimensional electron gas (2DEG) formation at the n-type LaO/TiO_2 terminated $SrTiO_3/LaAlO_3$ (STO/LAO) interface [1–6]. Only recently the 2D nature of the gas has been proved by Shubnikov–de Haas experiments [7]. Furthermore, recent work [8,9] emphasized the peculiar nature of the conductive sheet at the STO/LAO interface in comparison to that found at conventional semiconductor interfaces: extremely small thickness ($\sim$ nm rather than $\sim\mu$m), large binding energies (tenths of eV rather than meV), and correlated nature of the carriers (as opposed to nearly-free carriers), better described through the concept of two-dimensional electron liquid (2DEL). In experiment, extrinsic factors (La interdiffusion [10], O vacancies [11–13], surface adsorbates, ...) largely influence the observations, to the point that an intrinsic origin of the 2DEG in STO/LAO is still debated. In this Letter we demonstrate, based on advanced first-principles calculations appropriate for correlated systems, that the formation of the 2DEL can be explained by purely intrinsic mechanisms activated by the localized nature of Ti $3d$ t_{2g} carriers.

We investigate the ideal defect-free STO/LAO interface at varying interface charge density n_s (which, in our calculations, is the electron charge filling the Ti $3d$ conduction bands per interface unit area), from fully-compensated $1/2$ electrons$/A$ (where A is the 1×1 interface area) down to low carrier density. We find that for n_s lower than a threshold $n_c \sim 10^{14}$ cm^{-2}, the charge remains confined in an ultrathin ($\sim$ 1–2 nm) STO region. This confinement, or "self-trapping," is promoted by two intrinsic ingredients: the t_{2g} symmetry breaking induced by the interface crystal field, and the localized nature of $3d_{xy}$ states of Ti atoms adjacent to the interface. When n_s exceeds n_c, a portion of the charge spreads out over a slightly thicker STO region. Our results fully support the electronic origin scenario suggested by several experiments [8,9,14–16].

While previous theoretical works were based on conventional LDA/GGA [17–23] or parameter-dependent LDA + U [24–26], here we apply two advanced density-functional theory-based methods which provide an improved description of strongly correlated materials: the pseudo self-interaction corrected local-density functional (pSIC) [27], and the hybrid Fock-exchange plus Wu-Cohen GGA functional (B1-WC) [28]. Their performance for correlated oxides is demonstrated by many previous applications [27–29] and the correct description of bulk STO and LAO electronic structures. Technical details are described in the supplemental material [30].

We model the ideal, fully compensated (charged by $1/2$ electrons$/A$) STO/LAO interface [4] by a symmetric supercell with two identical TiO_2/LaO interfaces (see detail in supplemental material [30]). The half-electron redistribution near the interface is illustrated in Fig. 1(a), which reports the pSIC-calculated layer- and orbital-projected Ti t_{2g} density of states (DOS) in a small energy window near the STO conduction band bottom (the B1-WC results for the DOS, not displayed here, are quite similar). The corresponding band energies and Fermi surfaces, discussed later on, are reported in Figs. 2(a) and 2(c), respectively.

The interface crystal field splits the t_{2g} states in a lower d_{xy} singlet, and an upper d_{xz}, d_{yz} doublet inducing the preferential filling of the former, in agreement with measurements by x-ray spectroscopy [14] [see the corresponding band splitting in Fig. 2(a)]. Table I reports the (very consistent) B1-WC and pSIC values of singlet and doublet

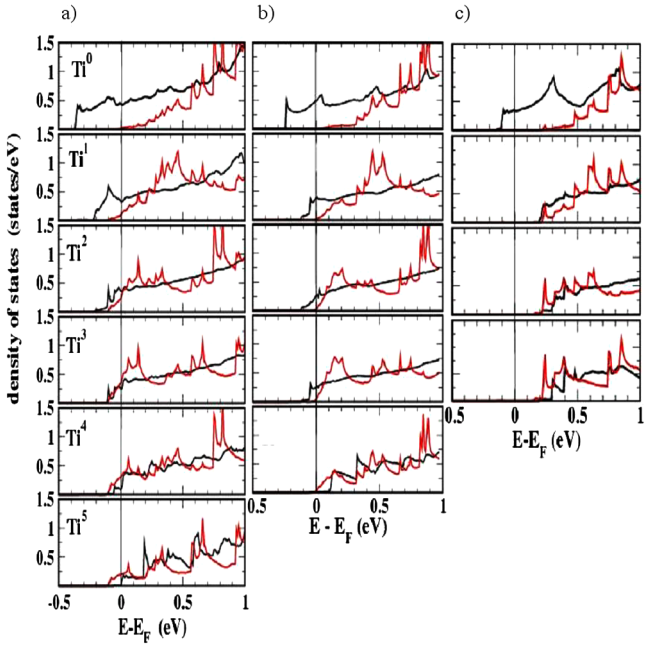

FIG. 1 (color online). Layer-projected and orbital-resolved density of states of the Ti $3d$ t_{2g} orbitals in the symmetric STO/LAO supercell calculated by pSIC. Black lines: d_{xy} singlet; red lines: (d_{xz}, d_{yz}) doublet; panels (a), (b), and (c) refer, respectively, to $n_s = 0.5$ electrons/A (i.e., 3.3×10^{14} cm^{-2}), 0.15 electrons/A (10^{14} cm^{-2}), and 0.03 electrons/A (0.2×10^{14} cm^{-2}). Ti^0 is the Ti atom at the interface, Ti^i the Ti atom of the ith layer below it. The e_g submanifold is empty and well above this energy range.

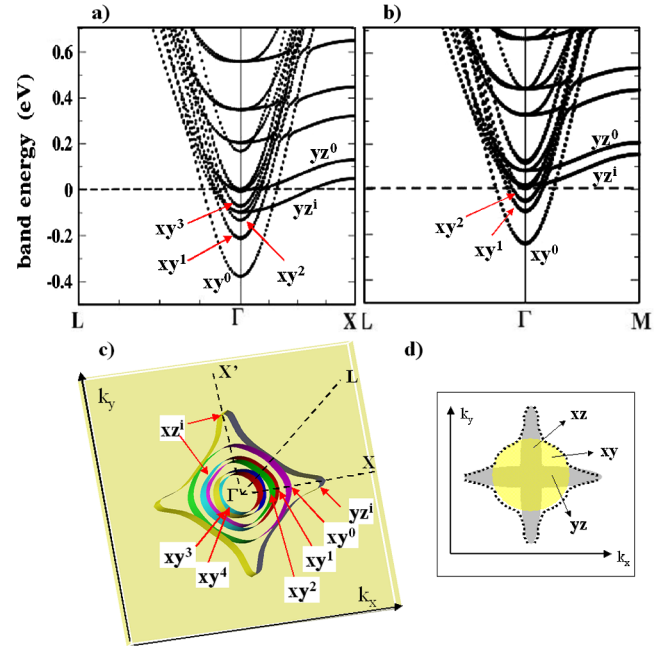

FIG. 2 (color online). Top: pSIC-calculated band energies for (a) $n_s = 0.5$ electrons/A (3.3×10^{14} cm^{-2}), and (b) $n_s = 0.15$ electrons/A (10^{14} cm^{-2}). Bottom: Panel (c) calculated Fermi surfaces for $n_s = 0.5$ electrons/A in the 1×1 Brillouin zone of edge $2\pi/a_{\mathrm{STO}}$; labels identify the dominant t_{2g} orbital character and the TiO_2 layer they belong to (same notations as in Fig. 1); notice that xz^i, yz^i, with $i \geq 1$ label the (nearly degenerate) occupied doublet orbitals located on Ti^1, Ti^2, etc. Panel (d) sketch of the calculated extremal Fermi surfaces (dotted black line) divided up into three contributions, the circular xy^0 and two cigar-shaped xz^i and yz^i bands.

occupations in each STO layer: a large charge fraction (0.15 electrons/A) sits in the d_{xy} state right at the interface (Ti^0); a much smaller and steadily decreasing portion also exists in the Ti^i d_{xy} states up to layer $i = 4$, until on Ti^5 no more d_{xy} charge is found. On the other hand, starting from Ti^1 a minor portion of charge is carried by interface-orthogonal d_{xz} and d_{yz} orbitals. This contribution, spread over a thicker STO region, survives beyond the sixth Ti layer below the interface. Concurrently, the singlet-doublet splitting decreases from ~0.37 eV for Ti^0 (0.4 eV according to B1-WC) to 0 at Ti^3, and then changes sign at Ti^4 as the singlet shifts above the doublet.

The 1/2 electrons/A (i.e., 3.3×10^{14} cm^{-2}) limit fixed by the polar catastrophe model is actually never reached in Hall measurements, which typically report n_s between 10^{13} cm^{-2} and 10^{14} cm^{-2}, depending on sample condition and preparation. This motivated us to investigate the 2DEL properties at lower charge carrier concentration (we do not address the reasons for a diminished charge density—trapping by defects, etc., ...—, which is immaterial for our present purpose). Thus, using the same structure, we fix n_s at two typical values: 10^{14} cm^{-2} (0.15 electrons/A) [9], and 0.2×10^{14} cm^{-2} (0.03 electrons/A) [3].

At $n_s = 10^{14}$ cm^{-2} [see the corresponding DOS and band energies in Figs. 1(b) and 2(b), respectively] E_F crosses four d_{xy} bands of the first four Ti atoms from interface, running just below the bottom of the doublet band manifold, which remains unoccupied. Thus, the charge is entirely localized within the first 1.5–2 nm from the interface and is exclusively of d_{xy} orbital character. Clearly, even a tiny increase of E_F would produce a charge spillout into the doublet states. The binding energy (i.e., the difference between the conduction band bottom at the interface and in the inner side of the slab) is 0.25 eV, thus quite smaller than the 0.37 eV for $n_s = 1/2$ electrons/A, and consistent with the experimental value of 0.25 ± 0.07 eV [31]. In the very

TABLE I. Orbital decomposition of the 1/2-electron charge on the STO side of the fully compensated n-type TiO_2/LaO interface calculated by pSIC and B1-WC (in parentheses). The TiO_2 layer labeled "Ti^5" is the farthest from the interface.

	d_{xy}		$d_{xz} + d_{yz}$		t_{2g}	
Ti^0	0.15	(0.15)	0	(0)	0.15	(0.15)
Ti^1	0.09	(0.09)	0.01	(0.01)	0.10	(0.10)
Ti^2	0.06	(0.05)	0.03	(0.02)	0.09	(0.07)
Ti^3	0.04	(0.04)	0.05	(0.04)	0.09	(0.08)
Ti^4	0	(0.01)	0.04	(0.05)	0.04	(0.06)
Ti^5	0	(0)	0.02	(0.02)	0.02	(0.02)
total	0.34	(0.34)	0.15	(0.14)	0.49	(0.48)

low-concentration case [see the DOS in Fig. 1(c)] all the charge is entirely localized on the Ti^0 d_{xy} orbital, and the binding energy is about 0.2 eV.

Our analysis reveals a moderately correlated nature of the confined charge: the energy splitting at the interface between d_{xy} and d_{xz}, d_{yz} directly controls the confinement extension. Standard LDA/GGA underestimates the splitting due to the poor treatment of the on-site Coulomb repulsion, while B1-WC and PSIC, appropriate for correlated electrons, restore the correct behavior [32]. We have estimated the contribution to the singlet-doublet splitting due to the on-site Coulomb repulsion to be ~0.2 eV at the interface layer for the $n_s = 1/2$ electrons/A case (see details in supplemental material [30]). This confining mechanism is fully consistent with that envisioned in Ref. [8], and it holds in general for both LAO films grown on STO or STO/LAO multilayers, irrespective of the presence or absence of built-in electric field in LAO (as confirmed by B1-WC calculations on isolated STO/LAO/vacuum stacks of various LAO thicknesses [33]).

Figure 3 summarizes the interface band lineup, charge profile, and binding energies obtained in our calculation. The confining potential for the d_{xy} charge (left, in yellow [light gray]) is just the interpolated profile of the conduction band bottom for the occupied d_{xy} states. A general relation between n_s and thickness of the metallic region is given in Fig. 3, right. Here $n_s(E_F)$ is calculated as the integral from band bottom to E_F of the DOS shown in Fig. 1(a), distinguishing total t_{2g} and d_{xy} contributions. The d_{xy} charge is extremely short range, peaking at Ti^0 and extending only up to five STO units; the (d_{xz}, d_{yz}) charge extends beyond the sixth STO layer below the interface. Despite the implicit rigid-band approximation, the plot

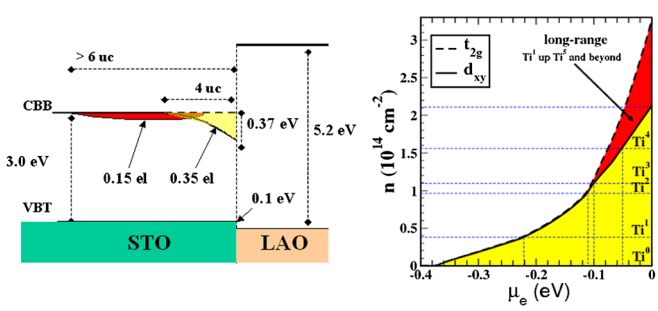

FIG. 3 (color online). Left: sketch of the band alignment at the LAO/STO interface as calculated in pSIC; yellow (light gray) and red (dark gray) areas indicate d_{xy} and $d_{xz} + d_{yz}$ contributions, respectively. Right: total t_{2g} (dashed) and d_{xy} (solid) charge densities per unit area as a function of chemical potential, calculated from the interface with 1/2 electrons/A assuming a rigid-band behavior ($E_F = 0$ corresponds to occupancy 1/2 electrons/A or 3.3×10^{14} cm^{-2}). Yellow (light gray) and red (dark gray) areas are contributions of planar d_{xy} and orthogonal (d_{xz}, d_{yz}) orbitals, respectively. On the right y axis, Ti^i indicates up to which Ti layer the d_{xy} charge (indicated by the dashed horizontal line) spreads.

interpolates well the charge redistribution for n_s calculated directly in Figs. 1(b) and 1(c): for n_s up to 0.4×10^{14} cm^{-2} the charge is entirely hosted by Ti^0 d_{xy}; above this value the Ti^1 d_{xy} state begins to fill as well. At $n_c \simeq 10^{14}$ cm^{-2} (0.15 electrons/A) even Ti^2 and Ti^3 d_{xy} states host some charge, while immediately above this level the charge spills onto d_{xz}, d_{yz} states, progressively acquiring a delocalized character. Hence, n_c represents the maximum concentration which can be accommodated exclusively by d_{xy} states, and is highly confined in a ~1.5–2 nm range from the interface.

We can use the model to analyze experimentally reported carrier densities. Several experiments (XAS [14], atomic force microscopy [34], hard x-ray photoemission [15,35]) report confinement regions of few nm, in line with our results. Huijben *et al.* [3] found for the STO/LAO superlattice a small $n_s \sim 0.2 \times 10^{14}$ cm^{-2} at $T = 0$ K, which according to our results should imply charge entirely localized within 1 nm from the interface. A similar value was reported by Thiel *et al.* [2] for the freestanding LAO film. Dubroka *et al.* [9] recently found $n_s = 0.9 \times 10^{14}$ cm^{-2}, that is near our critical n_c, and should imply a confinement length of 2 nm or so. In fact, the n_s profile measured by ellipsometry does decay sharply at about 2 nm, quite consistently with our calculated d_{xy} density profile. An additional tail, vanishing at 11 nm, with a fourfold reduced carrier density, could be reasonably associated with the extended d_{yz}, d_{xz} doublet charge (see populations in Table I).

We now come back to Fig. 2(c) to discuss the Fermi surface. We can distinguish five roughly circular Fermi sheets corresponding to the five Ti^i d_{xy} states ($i = 0, 4$) partially occupied at $n_s = 0.5$ electrons/A [Fig. 2(a)]. They are markedly parabolic in the (k_x, k_y) plane, and resemble closely their bulk counterparts. Contrariwise, d_{xz} and d_{yz} bands are quite anisotropic. The sketch in Fig. 2(d) illustrates how the largest Fermi surface for $n_s = 0.5$ electrons/A is in fact the intersection of d_{xz} and d_{yz} high-eccentricity ellipses with the circular d_{xy} section due to Ti^0. At lower $n_s = 0.15$ electrons/A (panel b), on the other hand, only circular d_{xy} sheets are occupied. The doublet bands, though, linger just above E_F, and small charge fluctuation may cause sloshing out of the 2 nm-wide confinement region.

The difference between singlet and doublet is also reflected in the calculated effective band mass m^*. For the d_{xy} bands, $m_x^* = m_y^* = 0.7$ (in units of m_e); for d_{xz} bands $m_x^* = 0.7$ and $m_y^* = 8.8$ (for d_{yz}, $m_x^* = 8.8$, $m_y^* = 0.7$ by symmetry). Thus, we are left with light electrons with $m_L^* = 0.7$ hosted by d_{xy} states, and heavy electrons with $m_H^* = 2(m_x^* m_y^*)/(m_x^* + m_y^*) = 1.3$ travelling within d_{xz} and d_{yz} states. They will contribute differently to mobility and transport. The ratio of conductivity due to d_{xy} carriers at Ti^0 to that of d_{xz}, d_{yz} electrons in their most populated layer (Ti^3) is $\sigma_0/\sigma_3 = n_0\, m_H^*/n_3 m_L^* \sim 5.6$, where n_0 and

n_3 are the calculated sheet densities for Ti^0 and Ti^3, respectively. Averaging over light and heavy carriers we obtain $m^* = n(m_L^* m_H^*)/(n_L m_H^* + n_H m_y^*) = 0.81$, with $n = (n_L + n_H) = 1/2$, and n_L and n_H the total charge of singlet and doublet states, respectively, (last row of Table I). Accounting for electron-phonon renormalization using a coupling constant $\lambda \sim 3$ typical for n-type STO [36], our estimate becomes $m_r^* = (1 + \lambda)m^* \simeq 3.2$, in agreement with that inferred from ellipsometry and transport [9], $m^* = 3.2 \pm 0.4$. Our interface band mass is only 25% larger than the corresponding STO bulk value: this is in line with recent observations [37] which found no thermopower enhancement in STO/LAO structures compared to STO bulk. Remarkably, the band shapes remain substantially unchanged with n_s; hence, planar mobility should not depend on carrier concentration in the intrinsic limit.

Finally, in view of the interest raised by spin-orbit coupling in recent magnetotransport experiments [38], we performed B1-WC calculations including spin-orbit coupling for the interface analyzed here. We only found a very marginal effect at the scale of the DOS analyzed in Fig. 1 (see supplemental material [30]). This clarifies that spin-orbit coupling, while playing an important role in field-effect phenomena, does not significantly affect the present discussion and conclusions.

In summary, using advanced first-principles methods, we provided an accurate description of the 2DEL at the intrinsic TiO_2/LaO interface of STO/LAO heterostructures. We find the 2D charge confinement as due to interface-induced Ti $3d$ state splitting and to the localized nature of the Ti $3d_{xy}$ states, thus supporting the experimental attribution [8,9,14] of 2DEL formation to a primarily electronic origin (possibly reinforced by interface-localized atomic displacements, see our supplemental material [30] and, e.g., the analysis of nonlinear dielectric response at the interface presented in Ref. [39]). Our results establish a relationship between sheet carrier density and spatial extension of the 2DEL, setting an intrinsic threshold ($n_c \sim 10^{14}$ cm^{-2} or 0.15 electrons/A) to the sheet carrier concentration of d_{xy} character that may be strictly localized near the interface; above this value, carriers start spilling over into the STO substrate. A connection between carrier density, binding energy, and thickness of the 2DEL is provided, which will be of practical guidance for future experiments and calculations.

Work supported by the European Union FP7 project OxIDes (Grant No. 228989), by MIUR PRIN 2008 project "2-DEG FOXI", by Fondazione BdS under a 2010 grant, by IIT Seed project NEWDFESCM, by the IAP Program P6/42 of the Belgian Science Policy, by the ARC project, TheMoTherm and by the EnergyWall project CoGeTher. Part of this work was carried out by A. F., V. F., and P. G. at the 2010 AQUIFER program of ICMR-UCSB in L'Aquila. Calculations performed at CASPUR Rome, Cybersar Cagliari, and Nic-3 at ULg.

[1] A. Ohtomo and H. Y. Hwang, Nature (London) **427**, 423 (2004).
[2] S. Thiel *et al.*, Science **313**, 1942 (2006).
[3] M. Huijben *et al.*, Nature Mater. **5**, 556 (2006).
[4] N. Nakagawa *et al.*, Nature Mater. **5**, 204 (2006).
[5] N. Reyren *et al.*, Science **317**, 1196 (2007).
[6] M. Huijben *et al.*, Adv. Mater. **21**, 1665 (2009).
[7] A. D. Caviglia *et al.*, Phys. Rev. Lett. **105**, 236802 (2010).
[8] M. Breitschaft *et al.*, Phys. Rev. B **81**, 153414 (2010); J. Mannarth and D. G. Schlom, Science **327**, 1607 (2010).
[9] A. Dubroka *et al.*, Phys. Rev. Lett. **104**, 156807 (2010).
[10] P. R. Willmott *et al.*, Phys. Rev. Lett. **99**, 155502 (2007).
[11] G. Herranz *et al.*, Phys. Rev. Lett. **98**, 216803 (2007).
[12] A. Kalabukhov *et al.*, Phys. Rev. B **75**, 121404 (2007).
[13] W. Siemons *et al.*, Phys. Rev. Lett. **98**, 196802 (2007).
[14] M. Salluzzo *et al.*, Phys. Rev. Lett. **102**, 166804 (2009).
[15] M. Sing *et al.*, Phys. Rev. Lett. **102**, 176805 (2009).
[16] A. Savoia *et al.*, Phys. Rev. B **80**, 075110 (2009).
[17] M. S. Park, S. H. Rhim, and A. J. Freeman, Phys. Rev. B **74**, 205416 (2006).
[18] Z. S. Popovic, S. Satpathy, and R. M. Martin, Phys. Rev. Lett. **101**, 256801 (2008).
[19] J.-M. Albina *et al.*, Phys. Rev. B **76**, 165103 (2007).
[20] K. Janicka, J. P. Velev, and E. Y. Tsymbal, Phys. Rev. Lett. **102**, 106803 (2009).
[21] J. Lee and A. A. Demkov, Phys. Rev. B **78**, 193104 (2008).
[22] U. Schwingenschlögl and C. Schuster, Europhys. Lett. **81**, 17 007 (2008).
[23] N. C. Bristowe, E. Artacho, and P. B. Littlewood, Phys. Rev. B **80**, 045425 (2009).
[24] R. Pentcheva and W. E. Pickett, Phys. Rev. B **74**, 035112 (2006); Phys. Rev. B **78**, 205106 (2008); Phys. Rev. Lett. **102**, 107602 (2009).
[25] Z. Zhong and P. J. Kelly, Europhys. Lett. **84**, 27001 (2008).
[26] S. S. A. Seo *et al.*, Phys. Rev. Lett. **104**, 036401 (2010).
[27] A. Filippetti and N. A. Spaldin, Phys. Rev. B **67**, 125109 (2003).
[28] D. I. Bilc *et al.*, Phys. Rev. B **77**, 165107 (2008).
[29] A. Filippetti and V. Fiorentini, Eur. Phys. J. B **71**, 139 (2009).
[30] See supplemental material at http://link.aps.org/supplemental/10.1103/PhysRevLett.106.166807 for technical details of the calculations and additional information.
[31] K. Yoshimatsu *et al.*, Phys. Rev. Lett. **101**, 026802 (2008).
[32] LDA predicts an interface singlet-doublet splitting significantly ($\sim$ 50%) smaller, and a localization length slightly longer, than in our approach. See, e.g., W.-j. Son *et al.*, Phys. Rev. B **79**, 245411 (2009).
[33] D. Fontaine, D. I. Bilc, A. Filippetti, P. Delugas, V. Fiorentini, and Ph. Ghosez (to be published).
[34] M. Basletic *et al.*, Nature Mater. **7**, 621 (2008).
[35] C. Cen *et al.*, Nature Mater. **7**, 298 (2008).
[36] J. L. M. van Mechelen *et al.*, Phys. Rev. Lett. **100**, 226403 (2008).
[37] I. Pallecchi *et al.*, Phys. Rev. B **81**, 085414 (2010).
[38] A. D. Caviglia *et al.*, Phys. Rev. Lett. **104**, 126803 (2010).
[39] O. Copie *et al.*, Phys. Rev. Lett. **102**, 216804 (2009).